Journal of Physics B:
Atomic, Molecular and
Optical Physics

PAPER • OPEN ACCESS

Dynamics of highly-ionized diiodomethane: Coulomb explosion, energy exchange and rotating fragments

To cite this article: F Trost *et al* 2025 *J. Phys. B: At. Mol. Opt. Phys.* **58** 085101

View the article online for updates and enhancements.

You may also like

- Depth-of-interaction encoding techniques for pixelated PET detectors enabled by machine learning methods and fast waveform digitization
Bing Dai, Srilalan Krishnamoorthy, Emmanuel Morales et al.
- Recent advancements in atomic many-body methods for high-precision studies of isotope shifts
B K Sahoo, S Blundell, A V Oleynichenko et al.
- Towards improved prescription metrics in novel radiotherapy techniques: a machine learning study
Alfredo Fernandez-Rodriguez and Yolanda Prezado

This content was downloaded from IP address 150.244.1.242 on 21/07/2025 at 09:18

OPEN ACCESS
IOP Publishing
Journal of Physics B: Atomic, Molecular and Optical Physics
J. Phys. B: At. Mol. Opt. Phys. **58** (2025) 085101 (10pp)
https://doi.org/10.1088/1361-6455/adc963

Dynamics of highly-ionized diiodomethane: Coulomb explosion, energy exchange and rotating fragments

F Trost[1,*], S Díaz-Tendero[2,3,4], H Lindenblatt[1], S Meister[1], K Schnorr[1,5], S Augustin[1,5], G Schmid[1], Y Liu[1], P Schoch[1], F Hosseini[6], M Zmerli[6], R Guillemin[6], M-N Piancastelli[6], M Braune[7], C D Schröter[1], T Pfeifer[1], F Martín[2,8], M Simon[6] and R Moshammer[1]

[1] Max Planck Institute for Nuclear Physics, Saupfercheckweg 1, 69117 Heidelberg, Germany
[2] Departamento de Química, Universidad Autónoma de Madrid, 28049 Madrid, Spain
[3] Institute for Advanced Research in Chemistry (IAdChem), Universidad Autónoma de Madrid, 28049 Madrid, Spain
[4] Condensed Matter Physics Center (IFIMAC), Universidad Autónoma de Madrid, 28049 Madrid, Spain
[5] Paul Scherrer Institut, Villigen 5200, Switzerland
[6] Sorbonne Université and CNRS, UMR 7614,Laboratoire de Chimie Physique-Matière et Rayonnement, F-75005 Paris, France
[7] Deutsches Elektronen-Synchrotron (DESY), Notkestraße 85, 22607 Hamburg, Germany
[8] Instituto Madrileño de Estudios Avanzados en Nanociencia (IMDEA-Nano), Campus de Cantoblanco, 28049 Madrid, Spain

E-mail: trost@mpi-hd.mpg.de

Received 30 December 2024, revised 7 March 2025
Accepted for publication 4 April 2025
Published 16 April 2025

Abstract

The dissociation dynamics of diiodomethane molecules (CH_2I_2) have been investigated following absorption of 98 eV XUV photons. In the measurement at the reaction microscope endstation at the free-electron laser FLASH2, ionic fragments created by 4d core ionization followed by Auger decay have been detected in coincidence. In the one-photon absorption channel $CH_2^+/I^+/I^+$, a concerted three-ion breakup and a sequential dissociation via a rotating intermediate CH_2I^{2+} ion have been identified. Classical simulations based on a Coulomb repulsion model and *ab initio* molecular dynamics in the frame of the Density Functional Theory have been performed. Both types of simulations reproduce different aspects of the observed fragmentation dynamics, in particular a delayed second bond break after dissociation of the first iodine ion. In the study of the potential energy surface we have located a minimum after the emission of the first I^+. We attribute the sequential mechanism to the trapping of the rotationally excited CH_2I^{2+} fragment in this transient intermediate, which corresponds to a potential energy well that protects it against the cleavage of the second C–I bond.

Keywords: molecular dynamics, ionization, free-electron lasers, diiodomethane, simulation, fragmentation

* Author to whom any correspondence should be addressed.

Original Content from this work may be used under the terms of the Creative Commons Attribution 4.0 licence. Any further distribution of this work must maintain attribution to the author(s) and the title of the work, journal citation and DOI.

© 2025 The Author(s). Published by IOP Publishing Ltd

1. Introduction

In the past decades, a number of variants of molecular dissociation dynamics have been identified in CH_2I_2. When irradiated with few-eV UV photons, dissociation into neutral CH_2I and I fragments can occur [1–3]. Detailed studies of the fragments' kinetic energies have concluded that the resulting CH_2I radical is in a highly excited rovibrational state [4, 5]. The dissociation process, however, was found to be fast compared to the CH_2I fragment's rotation period [1]. The process of an iodine atom separating from the CH_2I_2 molecule may occur via a transient isomer state (CH_2−I−I), according to calculations and experimental interpretations [6].

The process of halogen elimination has been detected in diiodomethane as well after absorption of UV-photons (two-photon excitation at 248 nm by [7] and single-photon excitation below 124 nm by [8]). It was found to be a fast dissociation (less than 50 fs) following three-photon excitation at 312 nm [9]. It has been reported that the dominant mechanism for the emission of molecular iodine I_2 from CH_2I_2 is, after two-photon excitation at 312 nm, a direct dissociation in which the two C–I bonds break at the same time (called concerted) [10]. In the same work, a different pathway was found to occur via an intermediate CH_2−I−I isomer state as well. This process is also concerted, but characterized by asynchronous breaking of the C–I bonds. The I_2 molecule from such an asynchronous fragmentation has been found to be in a highly excited rotational state [11, 12] following excitation by multi-photon absorption at 310–312 nm. The elimination of molecular halogens has also been observed in molecules containing halogens other than iodine when using lasers of the same wavelength [9, 11].

When exposed to XUV radiation of around 50 eV, the created $CH_2I_2^+$ ion has been observed to eject an iodine atom I or an iodine ion I^+ [13]. The atomic I-loss process has been found to happen either through direct cleavage of the C–I bond or, as was computationally shown, via an intermediate CH_2–I–I^+ isomer state [14] when the molecule is irradiated with 40 eV synchrotron radiation. The relevance of this isomer state for the dissociation process of the $CH_2I_2^+$ ion has been confirmed by transient absorption measurements at photon energies between 48 and 54 eV [15].

When entering the regime of multi-photon ionization, several electrons can be ejected from the molecule. The remaining molecular ion then dissociates mainly through electrostatic repulsion. The process of extracting information on the original molecular structure by analyzing the momenta of the fragment ions is called Coulomb explosion imaging (CEI) [16–18]. It is not only possible to use CEI to gain information on the molecular structure, but also to study the nature of the fragmentation process itself [19]. For example, by using CEI, the relative position and orientation of the two CO_2 molecules in a carbon dioxide dimer have been measured [20, 21]. In addition, it was determined that there are different competing dissociation processes [22]. A concerted dissociation that occurs in a single step leads to different relative momenta of the ionic fragments than a sequential process via an intermediate state.

Such different dissociation pathways have been identified in a number of three-atomic molecules, such as OCS [23], CO_2 [24, 25], SO_2 [26], and CS_2 [27]. In larger molecules more similar to diiodomethane studied in this experiment, very similar dissociation behaviour has been recorded, for example in $CHBr_3$ [28] and in C_3H_7I [29]. In each of these studies, the differentiation between the fragmentation pathways was achieved by ion-momentum correlation. A sequential dissociation pathway was isolated in all of these cases via an intermediary rotating molecular ion.

Recently, fragmentation of diiodomethane into three particles has been measured after strong-field ionization with an intense infrared laser pulse [30]. The three ionic coincident fragments detected there were CH_2^+ and two iodine ions of various charge states. Single-pulse measurements led to three-body fragmentation into the $CH_2^+/I^+/I^+$ coincidence channel where different fragmentation pathways have been identified, including a sequential pathway via an intermediary CH_2I^{2+} ion. This three-body dissociation dynamics has very recently been studied in CH_2ClBr as well [31].

Iodine atoms have a large absorption cross section for core ionization at photon energies of around 90 eV [32]. Therefore, the iodine atoms in the CH_2I_2 molecule act as efficient absorption sites for XUV radiation. The creation of a 4d-hole in an iodine atom causes subsequent relaxation dynamics including Auger decay [33]. The energy of a single XUV photon is sufficient to release a total of three electrons from a CH_2I_2 molecule through a cascade of two Auger decays. In this work, the detection of different fragmentation pathways leading to the $CH_2^+/I^+/I^+$ coincidence channel is described. We investigate the dynamics of this three-body fragmentation channel in the weak field regime by ionizing the CH_2I_2 molecule with a single XUV pulse; the dissociation processes were initiated by the absorption of a single 98 eV photon. The results of these measurements are compared with those previously reported in the strong field regime. We experimentally determined the three-dimensional momenta of all fragment ions. In this kinematically complete analysis, we identified a concerted three-ion fragmentation and a sequential pathway via a rotating intermediate CH_2I^{2+} molecular ion. We infer and interpret these measurements with molecular dynamics simulations performed with density functional theory (DFT) and classical models based on Coulomb repulsion.

2. Methods

2.1. Experimental setup

The experiment was conducted at the atomic physics endstation at the free- electron laser FLASH2 in Hamburg. A detailed description of the experimental setup can be found in [34]. In brief, the endstation consists of a reaction microscope, a supersonic gas jet for target delivery, and an in-line XUV optics

system. FLASH2 is an XUV free-electron laser (FEL) that provided light pulses at 98 eV photon energy with a duration of approximately 50 fs. The intensity in the focus region is estimated to be $3 \times 10^{15}\,\mathrm{W\,cm^{-2}}$.

In the reaction microscope, the interaction of the XUV pulses with the target molecules creates ions which are accelerated to a time- and position-sensitive detector via a homogeneous electric field. There is no drift region. The time-of-flight and the two-dimensional impact position on the detector are recorded. From this information, the three-dimensional ion momenta immediately after the molecular dissociation can be reconstructed. The detector is capable of registering multiple ions from the same XUV pulse. Through this coincidence measurement it is possible to detect all ions originating from the dissociation of a single molecule.

For the coincidence analysis, the separate ion species have been identified by their respective time-of-flight windows. A set of three ions ($CH_2^+/I^+/I^+$) is detected 'in coincidence' if all ions originated from an interaction with the same FEL pulse and the sum of their momenta is close to zero for each of the three spatial dimensions x, y, and z. To ensure this, three separate momentum-sum conditions have been applied, one for each dimension.

2.2. Computational details

2.2.1. Quantum chemistry calculations. Molecular dynamics (MD) simulations were performed using the atom centered density matrix propagation model (ADMP) [35–37]. ADMP is an extended Lagrangian MD method, in which the electronic degrees of freedom are propagated by introducing a fictitious term in the Lagrangian. In this approach, the forces acting on the five atoms (one carbon, two hydrogen, and two iodine atoms) are derived computing on-the-fly the electronic ground-state potential-energy surface. The atoms' positions and velocities are then propagated classically through time according to the resulting inter-atomic/-molecular forces. In this case, the potential energy was computed using the DFT, in particular with the B3LYP [38–41] functional, in combination with a SDD basis set, which includes the Dunning/Huzinaga full double zeta basis [42] for C and H atoms and the Stuttgart/Dresden effective core potentials basis set for the I atom [43]. To mimic the experimental conditions, the dynamics of the triply-ionized molecule was propagated starting from the optimized geometry of the neutral ground state, thus assuming a sudden ionization in a Franck–Condon approximation. The initial excitation energy was randomly distributed among the nuclear degrees of freedom. Therefore, we consider that after the 4d core photoionization followed by Auger decay, the tricationic state is created with some internal excitation energy which is rapidly redistributed among the nuclear degrees of freedom. In the simulations we have considered electronic states with doublet and quadruplet spin multiplicity and, in each case, we have performed MD simulations scanning the internal excitation energy between 1 and 5 eV. To ensure adiabaticity in the trajectories we set a time step of $\Delta t = 0.1$ fs and a fictitious electron mass of $\mu = 0.1$ amu. The trajectories were propagated up to $t_{\max} = 2$ ps.

Explorations of the potential energy surface (PES) were carried out at the same level of theory, B3LYP/SDD. Both in the PES exploration and in the MD simulations, we considered the doublet and the quadruplet spin multiplicity. All calculations were performed using the Gaussian16 program [44].

The computational strategy followed here was successfully used to disentangle the fragmentation dynamics of ionized and excited molecules and molecular clusters in the gas phase (see e.g. [45–51]).

2.2.2. Classical simulation. Simulations on the basis of a Coulomb repulsion model have been performed as a second independent approach to better understand the momentum correlations detected in the experiment. The ions (two I^+ and one $CH_2{}^+$) are represented as point charges with respective masses that repel each other by their Coulomb force. In addition, a Lennard-Jones (LJ) potential [52] is simulated between the $CH_2{}^+$ ion and one of the I^+ ions to bind them together. The LJ potential has the following form:

$$V_{\mathrm{LJ}}(r) = 4\epsilon\left[\left(\frac{\sigma}{r}\right)^{12} - \left(\frac{\sigma}{r}\right)^{6}\right]. \tag{1}$$

Here ϵ is the maximum depth of the potential and σ is the distance at which the potential is zero. This additional potential is switched off after a pre-defined lifetime during the simulation in order to simulate the secondary dissociation of the CH_2I^{2+} ion. Since the charges are placed at the positions of the ions, the charge distribution in the simulated CH_2I^{2+} intermediate molecular ion is $+1$ at the iodine and $+1$ at the CH_2 group. The simulation is run 50 000 times with an exponential distribution of the lifetime of the LJ potential. The initial condition takes the ground-state geometry of the molecule [53] and varies the positions of all three ions by a random two-dimensional Gaussian distribution with a standard deviation of 5 pm. The initial velocities are set to zero.

The parameter σ of the LJ potential was set such that the potential minimum agrees with the C–I bond length. The potential depth ϵ was chosen to be 0.2 au (5.4 eV). Together with the repelling Coulomb potential of the I^+ and $CH_2{}^+$ ions, the depth of the combined potential is 0.09 au (2.4 eV) which is approximately the dissociation energy of a C–I bond in a neutral molecule [54]. The depth of the LJ potential was found to have no effect on the nature of the resulting momentum distribution, if it is deep enough. If the LJ potential is too shallow, the change in electrostatic potential energy caused by the randomized distribution of the initial positions of the ions can cause early dissociation, before the deactivation of the LJ potential. The chosen value of 0.2 au (5.4 eV) was found to be well below this threshold when combined with the repelling Coulomb potential. For this reason, together with having the combined LJ and Coulomb potential approximate the dissociation energy of a C–I bond, this value for the potential depth of the simulated LJ potential was chosen.

3. Results and discussion

In this measurement, the coincidence channel $CH_2^+/I^+/I^+$ is the most prevalent among the three-ion coincidences. The detection rate declines sharply towards higher charge states of the iodine ions. This work only includes events in which the CH_2^+ group stays intact. Due to background from dissociating hydrogen molecules in the interaction chamber, it was not possible to resolve coincidences where H^+ ions separated from the diiodomethane molecule.

The creation of the three ions I^+, I^+, and CH_2^+ from a diiodomethane molecule is mostly a single-photon process. If a second photon was involved, the charge states of the emerging ionic fragments are expected to be higher than 1+. It is possible to reach a triply-ionized state by the absorption of two photons (core ionization followed by Auger decay and subsequent valence ionization, or vice versa), but this is very unlikely because the cross-section for valence ionization at the photon energy of 98 eV is much smaller than for core ionization [32, 55]. In addition, intensity dependence of the ion yield confirms that the observed fragmentations are caused by single-photon absorption.

For analyzing and displaying the momentum correlation between the three ions, a Newton plot is used. This is a common method of representation for momenta of three-body dissociations. Due to momentum conservation, the momenta of all three ions are always found in one common plane. Therefore, the set of three momenta can be collectively rotated into the *xy*-plane of the Newton plot. This is usually done such that the momentum of a specific ion species (in this case the CH_2^+ ion) is oriented along the positive *x*-axis. The momentum of the CH_2^+ ion is, however, not shown in the Newton plot. It is only used for the alignment purpose. An entry is made in the Newton plot for each of the other two ions' momenta in the *xy*-plane; one in the top half and one in the bottom half of the histogram. When this is done for multiple independent dissociation events, the emerging structure in the Newton plot contains information about the momentum correlation between the three ions.

Figure 1 shows the Newton plot of the $CH_2^+/I^+/I^+$ dissociation channel measured in this work. The momentum vector of the CH_2^+ fragment is oriented along the positive *x*-axis. A histogram of the CH_2^+ momentum is shown in the inset. The coincidence ion detection method cannot differentiate between the two identical I^+ ions with regard to their role in the dissociation process. For this reason, each iodine momentum was plotted once in the upper and once in the lower half of the Newton plot. Therefore, the momentum correlation displayed in the Newton plot is symmetric with regard to the *x*-axis.

The momentum correlation between the three ions displays several features. The two most prominent ones are an inner-oval shape (region A) in figure 1 with maxima at the upper and lower part at around ±190 au and an outer, much weaker structure of two intersecting rings (region B), one left and one right of the central oval. The kinetic energy of the CH_2^+ fragment

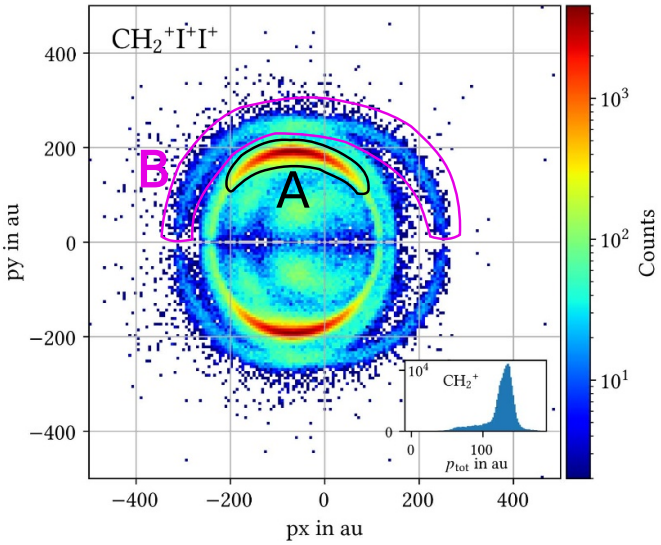

Figure 1. Newton plot of the measured one-photon dissociation of CH_2I_2 into CH_2^+, I^+, and I^+. The CH_2^+ momentum (not shown) is aligned along the positive *x*-direction. The inset shows the total momentum spectrum of the CH_2^+ species. As positive and negative transverse momenta (p_y) of the iodine atom with respect to the CH_2 fragment cannot be distinguished, the plot was symmetrized accordingly. The two indicated regions (A in black, B in magenta) correspond to the momentum correlations of different dissociation mechanisms.

is, on average, lower for feature B than for feature A. The feature close to the center of the inner-oval shape corresponds to low-momentum ions, both I^+ and CH_2^+. It probably originates from a fragmentation channel that differs from the concerted and sequential pathways described in this work and poses an interesting topic for further analysis and experiments.

Regarding the origins of the features A and B described above, a deep analysis using different theoretical methods was carried out in order to gain insight into the nature of these momentum correlation features.

MD simulations using the ADMP method were performed with internal energies in the range from 1 to 5 eV, including doublet and quadruplet spin multiplicity and with a total of 2560 trajectories. The analysis of the fragmentation channels populated in such trajectories was performed after 2 ps of propagation. A summary of the computed results is given in figure 2. The dominant channel at low internal energy corresponds to the cleavage of one C–I bond. From 3 eV on, loss of the second I atom appears, becoming dominant at 5 eV. Other minor channels with the loss of an H atom are also observed, but with probabilities smaller than ∼10% in the energy range considered. Oscillations in the most populated channels are due to the lack of statistics at low excitation energies.

At the end of each simulated trajectory, the momenta of the iodine nuclei and the methylene group are computed and displayed in a Newton plot in the same way as the experimental data. The resulting histogram is shown in figure 3. The momenta displayed there have been computed with internal energies of 3 eV and 5 eV, as the most representative of the fragmentation dynamics.

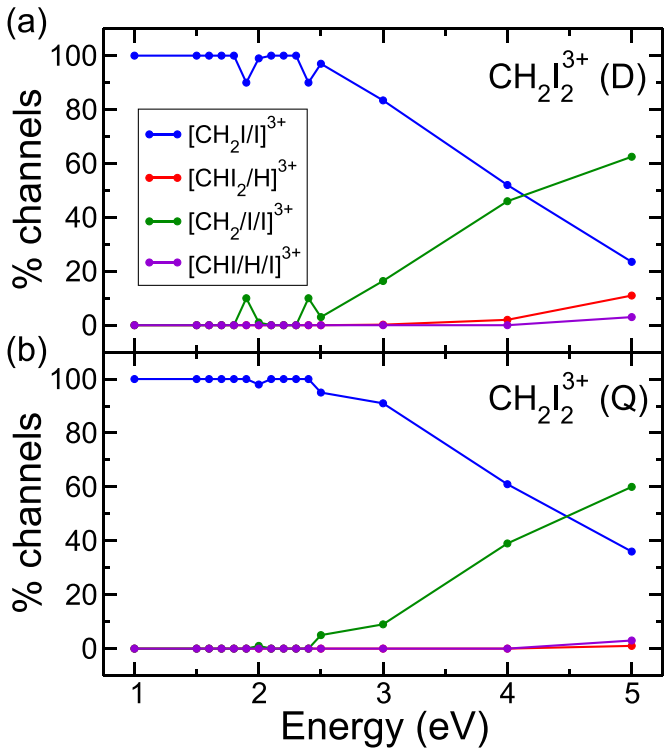

Figure 2. Percentage of fragmentation channels as a function of the internal excitation energy computed in the molecular dynamics simulations using the ADMP method. Results for the triply-ionized diiodomethane with (a) doublet $CH_2I_2^{3+}$(D) and (b) quadruplet $CH_2I_2^{3+}$(Q) spin multiplicity.

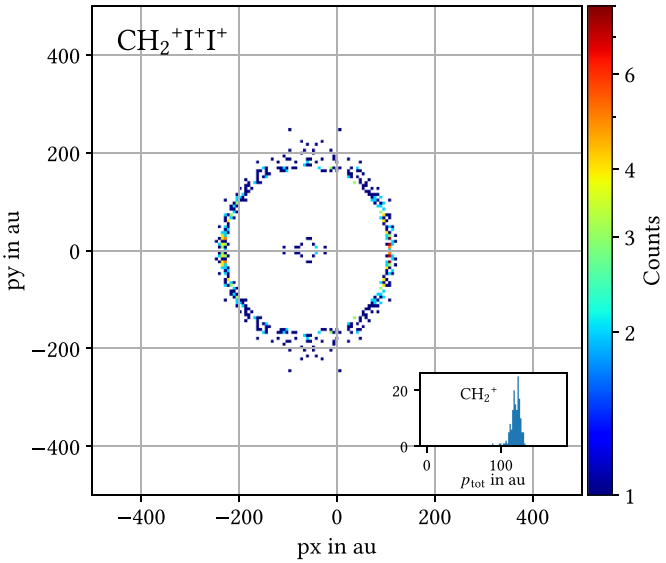

Figure 3. Newton plot of the triple-ion coincidence channel $CH_2^+/I^+/I^+$ as simulated with the ADMP model. The initial excitation energies of 3 eV and 5 eV are combined, the simulation duration is 2 ps with a 0.1 fs time step. The momenta of the hydrogen atoms and the carbon atom are added up to obtain the momentum of the CH_2^+ group, shown in the inset. The momentum of the methylene group (not plotted) is oriented along the positive *x*-axis.

The Newton plot of the ADMP simulated fragmentation processes shows a prominent ring structure. Regarding size and shape, this ring is similar to the central oval feature seen in the measurement data. However, the most striking difference is that the simulation does not reproduce the maxima at high and low *y*-momentum values.

The low-momentum feature close to the center of the ring structure originates from a small fraction of trajectories where the two iodine atoms did not separate from each other.

The question of why the ADMP simulation produces this particular momentum distribution can be answered by looking at the lifetimes of the CH_2I intermediate molecule in this simulation. The mean value of its lifetime distribution is 60 fs with a maximum value of 231 fs, while underrepresenting very short lifetimes below approximately 10 fs. That means that the ADMP simulation covers exclusively the intermediate range of CH_2I lifetimes. Therefore, there is always enough time for at least a partial rotation of the CH_2I molecule, which causes the momentum correlation feature A (seen in the experiment) to not appear in the ADMP simulation. Feature B, indicating the sequential dissociation with much longer lifetimes of the intermediate state, does also not occur in the ADMP simulation. What is left is the momentum correlation indicative of exclusively intermediate lifetimes (the closed inner-ring feature) without the feature originating from very short lifetimes (the maxima at high and low *y*-momentum, representing the original molecular structure).

In the top and bottom part of the Newton plot, the ADMP simulation results indicate that the iodine dissociation times are longer than average. In this region, the ring structure appears less clear. Instead, it more resembles the intersection of the two outer rings seen in the measured momentum correlation. This suggests that simulation of intermediate states with even longer lifetime could lead to a representation reminiscent of this double ring structure.

The simulated changes in molecular geometry are sketched in figure 4. It can be seen that the first iodine atom leaves the molecule while the methylene group starts to rotate around the other iodine nucleus, forming an intermediate CH_2I state.

The ADMP simulation successfully reproduces the inner-oval part of the measurement which is caused by rather quickly dissociating molecules. The Newton plot also suggests that longer-living states play an important role in the dissociation dynamics. It is also clear from this simulation that longer-living states could play an important role in explaining the measured ion momentum correlation of feature B. To further investigate these intermediate rotating states, a classical simulation has been performed. The classical simulation approach to gain insight into the fragmentation process was chosen because it is conceptually easier and requires fewer computing resources compared to the ADMP simulation.

In figure 5, the simulated Newton plots using the classical MD are presented. The timescale for the LJ potential lifetime distribution is 2 fs for figure 5(a), 10 fs for figure 5(b), and 5000 fs for figure 5(c).

For very short time spans between the ejection of the two iodine ions from the molecule, the ground-state geometry has very little time to change and the two maxima in the resulting

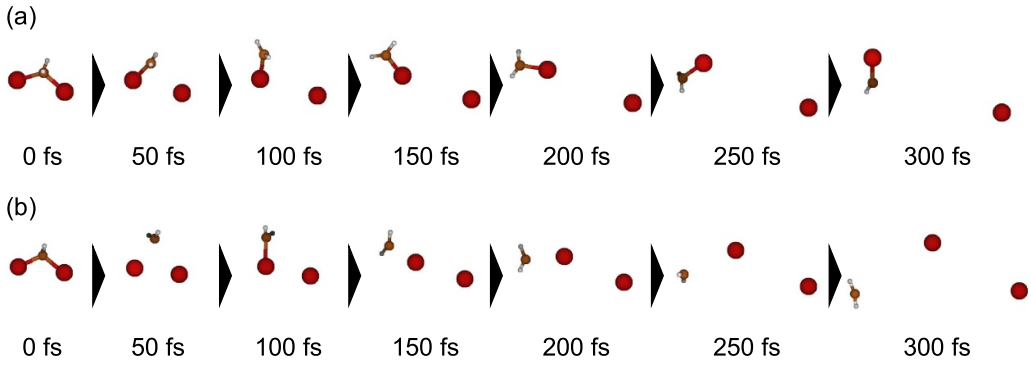

Figure 4. Sphere model of molecular geometry at different times during the ADMP simulation for two example trajectories. (a): 1 eV initial energy. The initial separation of the molecule into CH_2I and I is visible, but the rotating CH_2I fragment stays intact. (b): 3 eV initial energy. The CH_2I fragment rotates and after $\sim$ 250 fs it dissociates into CH_2 and the second I atom.

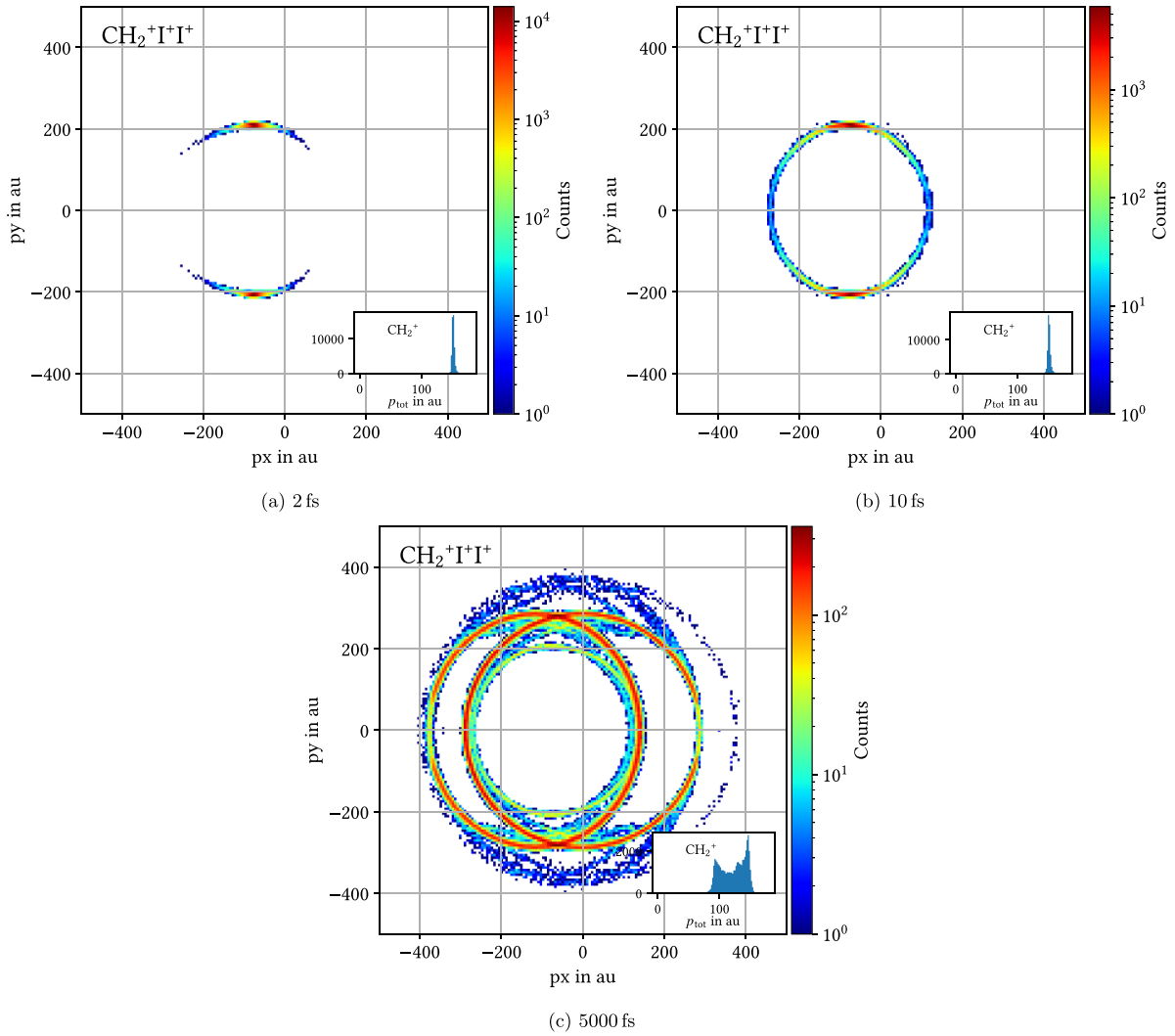

Figure 5. Newton plots of classically simulated fragmentation with different lifetimes for the binding potential. Its exponential distribution has a lifetime mean value of (a) 2 fs, (b) 10 fs, and (c) 5000 fs. The three ions repel each other by their Coulomb force. The momentum of the CH_2^+ ion is oriented along the positive x-axis (not plotted). Histograms of the CH_2^+ momentum are shown in the insets. The variation in the ion momenta is the result of varying initial positions as well as varying the lifetime of the binding LJ potential.

Newton plot in figure 5(a) again mirror the original orientation of the ions. This very fast double-ejection channel is thus consistent with the experimentally measured signal in region A of figure 1.

When there is a LJ potential with an average lifetime of 10 fs, the resulting momentum correlation in figure 5(b) still shows the two prominent maxima, but also displays a closed ring structure. This is similar to the inner-oval shape of the measured momentum correlation in figure 1 as well as the Newton plot of the ADMP simulation in figure 3.

For the simulation of long lifetimes of the LJ potential, the CH_2I^{2+} intermediate ion stays intact on a picosecond timescale before it fragments into the I^+ and $CH_2{}^+$ ion pair. During this time, it completes several rotations with regard to the ejection direction of the first I^+. This rotation is, in this classical simulation, introduced by the Coulomb repulsion from the first I^+ leaving the molecule. The resulting momentum correlation, shown in the Newton plot in figure 5(c), consists of two large intersecting rings of the same size. An inner, less prominent ring is visible which corresponds to the previously described structure originating from fast dissociations. However, with a time scale of 5000 fs, only a small fraction of cases fragments in less than a few tens of femtoseconds, which is why the inner-ring structure is much less prominent here.

There is an additional weak feature in the simulated Newton plot for long CH_2I^{2+} lifetimes which can be seen at *y*-momenta close to ±400 au. Such high-momentum I^+ ions are the result of the $CH_2{}^+$ ion from the intermediate CH_2I^{2+} being ejected into the same direction as the I^+ from the first dissociation step. In those rare cases, the $CH_2{}^+$ ion spends a larger amount of time between the two iodine ions which, through Coulomb repulsion, leads to an increased momentum of the I^+ fragments. In the experiment, these weak features are not observed. The reason for this is that, in the classical simulation, the rotation axis of the CH_2I^{2+} molecular ion is always perpendicular to the direction in which the first I^+ leaves the molecule. This idealized situation is in reality almost never the case which makes the ejection of the $CH_2{}^+$ ion in the same direction as the first I^+ ion even more improbable than in the classical simulation.

Comparing the three cases of classically simulated molecular dissociation time scales with the measured momentum correlation, both the inner-oval shape with the strong maxima as well as the weak outer rings can be reproduced. This leads to the conclusion that there are at least two competing dissociation pathways present in the fragmentation of the diiodomethane molecule. The fast, concerted pathway is characterized by the ejection of two iodine ions in quick succession. Because the molecule's ground-state geometry is largely preserved in this case, the resulting momentum correlation reflects the ions' initial positions. The result in the Newton plot is the two prominent maxima at high and low *y*-momenta. The second identified dissociation pathway is characterized by a larger time span between the ejection of the two iodine ions and is called the sequential pathway. This time span between the two dissociation steps must be long enough such that the emission directions of the two I^+ are no longer correlated. The rotation period of the intermediary CH_2I^{2+} ion must therefore be shorter than its average lifetime. Only then the momenta of the two iodine ions are no longer correlated which is represented by the outer rings (region B) in the measured Newton plot.

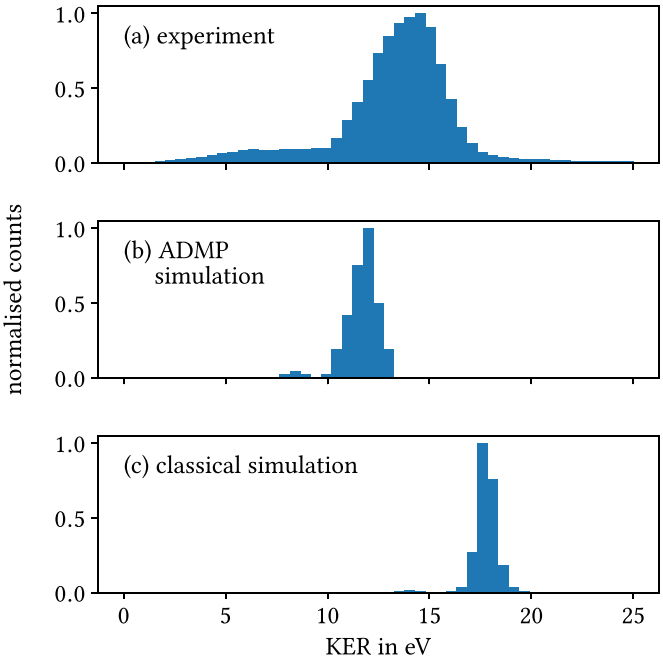

Figure 6. Comparison between the kinetic energy release (KER) of (a) the experimental data, (b) the ADMP simulation, and (c) the classical simulation. In the case of the classical simulation, all three lifetime cases have been combined.

The kinetic energy release (KER) of the molecular fragmentation is displayed in figure 6 for the three cases of (a) the experiment, (b) the ADMP simulation, and (c) the classical simulation, where all three cases for the lifetime of the CH_2I^{2+} intermediate state have been aggregated. The KER obtained from the experimental data shows a much broader distribution than is the case for both simulations. The Coulomb model overestimates the KER, which is not unusual when internal excitations are only addressed in a rudimentary way. The ADMP simulation, on the other hand, underestimates the KER compared to the experiment.

Further insights on the fragmentation were obtained with the exploration of the PES of $CH_2I_2{}^{3+}$ with doublet and quadruplet spin multiplicity, computed using the DFT. Figure 7 shows the triple ionization threshold and the fragmentation pathways towards the most populated channels, experimentally measured and computed with the MD simulations. From the ground state of the neutral diiodomethane, CH_2I_2(S), vertical ionization towards triply-ionized diiodomethane with doublet $CH_2I_2{}^{3+}$(D) and quadruplet $CH_2I_2{}^{3+}$(Q) spin multiplicity is considered. In the PES of the quadruplet, direct fragmentation with the loss of the first iodine atom occurs. A very shallow minimum is located on the PES of the doublet spin, with a tiny energy barrier before leading to fragmentation, which is negligible. In both cases, we can consider that dissociation towards channel CH_2I^{2+} /I^+ is a spontaneous process. However, further fragmentation of the remaining CH_2I^{2+}

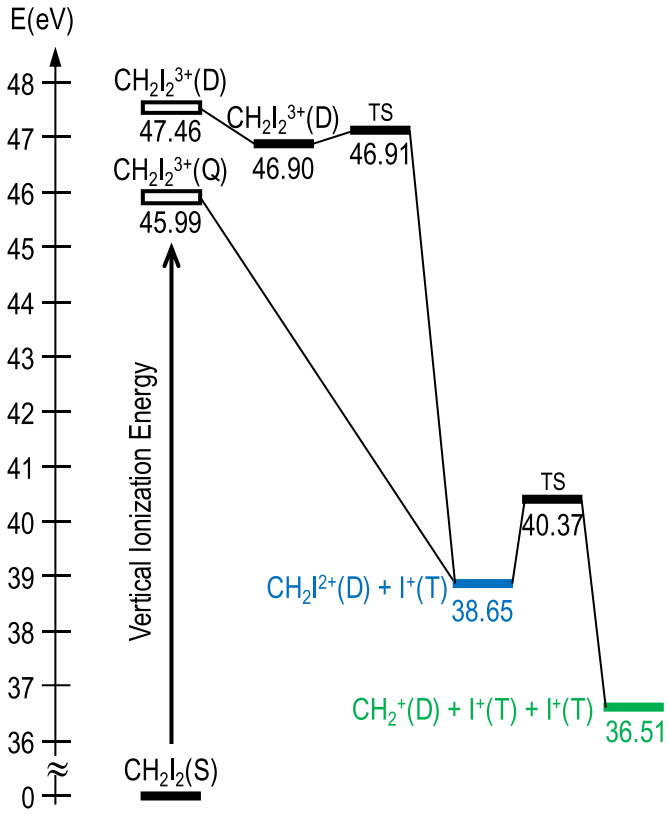

Figure 7. Relevant points in the potential energy surfaces of triply-ionized diiodomethane with doublet $CH_2I_2^{3+}$(D) and quadruplet $CH_2I_2^{3+}$(Q) spin multiplicity. Vertical ionization of the neutral ground state, with singlet spin multiplicity CH_2I_2(S). Relative energies, given in eV and computed at the B3LYP/SDDall level of theory including zero point energy correction, are referred to neutral diiodomethane. The most stable multiplicity for each fragment is used: S—singlet, D—doublet, T—triplet and Q—quadruplet.

moiety, losing the second I^+ ion, is a process that shows a barrier of ∼1.7 eV. Therefore, in situations where the internal energy of the fragment CH_2I^{2+} is not sufficient, or is concentrated only in the rotational degrees of freedom, further fragmentation will not take place. In the case where there is a redistribution of the internal energy of the fragment sufficient to overcome the barrier, such fragmentation will be sequential, i.e. with a delayed emission of the second I^+ ion. Therefore, we can interpret the results discussed above, and explain why a fragment is trapped in a kind of rotational resonance. Finally, only if the internal excitation energy remaining after triple ionization is very large, direct fragmentation towards the $CH_2^+/I^+/I^+$ channel will be observed.

The results presented here provide the first observation of the fragmentation dynamics of the CH_2I_2 molecule following core ionization. A previous study has shown that diiodomethane molecules exposed to a single strong-field laser pulse exhibit both concerted and sequential fragmentation pathways [30], consistent with the findings reported here. The observation of these two fragmentation pathways in both strong-field laser ionization and XUV core ionization suggests that the fundamental principles governing molecular dissociation are largely independent of the excitation method. Further work, both experimental and theoretical, is required to better understand the nuances of these fragmentation pathways. In particular, understanding the factors that determine the branching ratio of the fragmentation processes and the mechanisms governing the lifetime and spontaneous dissociation of the intermediary CH_2I^{2+} molecular ion would provide valuable insights.

4. Conclusions

In summary, by a combination of experiment and simulations, we identified two different pathways in the dissociation of diiodomethane after ionization by a single XUV photon. One is a fast and concerted fragmentation into three singly-charged ions. The other is a sequential process via a rotating intermediate CH_2I^{2+} molecular ion. The dissociation of this intermediate ion occurs spontaneously and on a timescale that is longer than its rotation period.

Author contributions

The experiment was conceived by H L, S M, R M, G S, M S, and F T. The experimental setup was prepared by S A, M B, H L, S M, G S, K S, C D S, and F T. The experiment was conducted by S A, M B, R G, F H, H L, Y L, S M, R M, M-N P, K S, P S, M S, F T, and M Z. The data was analysed by R G, H L, S M, R M, M S, and F T. Interpretation and discussion of the results was done by S A, R G, H L, S M, R M, T P, K S, M S, and F T. The ADMP simulation was performed by S D-T. and F M. The classical simulations were conducted by H L and F T. The manuscript was written by S D-T and F T with contributions from S A, H L, F M, R M, T P, K S, and M S.

Data availability statement

The data cannot be made publicly available upon publication because no suitable repository exists for hosting data in this field of study. The data that support the findings of this study are available upon reasonable request from the authors.

Acknowledgments

We acknowledge the generous allocation of computer time at the Centro de Computación Científica at the Universidad Autónoma de Madrid (CCC-UAM). This work was partially supported by the MICINN—Spanish Ministry of Science and Innovation—Projects PID2022-138470NB-I00 and PID2022-138288NB-C31 funded by MCIN/AEI/10.13039 /501100011033, the Severo Ochoa Programme for Centres of Excellence in R & D (CEX2020-001039-S) and the María de Maeztu Programme for Units of Excellence in R & D (CEX2023-001316-M).

We acknowledge DESY (Hamburg, Germany), a member of the Helmholtz association HGF, for the provision of experimental facilities. Parts of this research were carried out at FLASH and we would like to thank the whole FLASH team for its support. Beamtime was allocated for proposal F-20171085 EC.

ORCID iDs

F Trost https://orcid.org/0000-0001-7756-286X
S Díaz-Tendero https://orcid.org/0000-0001-6253-6343
H Lindenblatt https://orcid.org/0000-0003-1728-7979
S Augustin https://orcid.org/0000-0003-1283-331X
P Schoch https://orcid.org/0000-0003-1462-4589
T Pfeifer https://orcid.org/0000-0002-5312-3747
F Martín https://orcid.org/0000-0002-7529-925X
M Simon https://orcid.org/0000-0002-2525-5435

References

[1] Kawasaki M, Lee S J and Bersohn R 1975 Photodissociation of molecular beams of methylene iodide and iodoform *J. Chem. Phys.* **63** 809–14
[2] Pence W H, Baughcum S L and Leone S R 1981 Laser UV photofragmentation of halogenated molecules. selective bond dissociation and wavelength-specific quantum yields for excited I($^2P_{1/2}$) and Br($^2P_{1/2}$) atoms *J. Phys. Chem.* **85** 3844–51
[3] Xu H, Guo Y, Liu S, Ma X, Dai D and Sha G 2002 Photodissociation dynamics of CH_2I_2 molecules in the ultraviolet range studied by ion imaging *J. Chem. Phys.* **117** 5722–9
[4] Kroger P M, Demou P C and Riley S J 1976 Polyhalide photofragment spectra. i. two-photon two-step photodissociation of methylene iodide *J. Chem. Phys.* **65** 1823–34
[5] Baughcum S L and Leone S R 1980 Photofragmentation infrared emission studies of vibrationally excited free radicals CH_3 and CH_2I *J. Chem. Phys.* **72** 6531–45
[6] Chen S-Y, Tsai P-Y, Lin H-C, Wu C-C, Lin K-C, Sun B J and Chang A H H 2011 I_2 molecular elimination in single-photon dissociation of CH_2I_2 at 248 nm by using cavity ring-down absorption spectroscopy *J. Chem. Phys.* **134** 034315
[7] Fotakis C, Martin M and Donovan R J 1982 Ultraviolet laser multiphoton excitation of CH_2I_2 *J. Chem. Soc., Faraday Trans.* **2** 1363–71
[8] Okabe H, Kawasaki M and Tanaka Y 1980 The photodissociation of CH_2I_2: Production of electronically excited I_2 *J. Chem. Phys.* **73** 6162–6
[9] Marvet U, Zhang Q, Brown E J and Dantus M 1998 Femtosecond dynamics of photoinduced molecular detachment from halogenated alkanes. I. Transition state dynamics and product channel coherence *J. Chem. Phys.* **109** 4415–27
[10] Marvet U and Dantus M 1996 Femtosecond observation of a concerted chemical reaction *Chem. Phys. Lett.* **256** 57–62
[11] Zhang Q, Marvet U and Dantus M 1997 Concerted elimination dynamics from highly excited states *Faraday Discuss.* **108** 63–80
[12] Zhang Q, Marvet U and Dantus M 1998 Femtosecond dynamics of photoinduced molecular detachment from halogenated alkanes. ii. asynchronous concerted elimination of I_2 from CH_2I_2 *J. Chem. Phys.* **109** 4428–42
[13] Wei Z, Li J, Zhang H, Lu Y, Yang M and Loh Z-H 2019 Ultrafast dissociative ionization and large-amplitude vibrational wave packet dynamics of strong-field-ionized di-iodomethane *J. Chem. Phys.* **151** 214308
[14] Cartoni A, Casavola A R, Bolognesi P, Borocci S and Avaldi L 2015 VUV photofragmentation of CH_2I_2: The $[CH_2I–I]^{\cdot+}$ iso-diiodomethane intermediate in the I-loss channel from $[CH_2I_2]^{\cdot+}$ *J. Phys. Chem.* A **119** 3704–9
[15] Rebholz M *et al* 2021 All-XUV pump-probe transient absorption spectroscopy of the structural molecular dynamics of di-iodomethane *Phys. Rev.* X **11** 031001
[16] Kanter E P, Cooney P J, Gemmell D S, Groeneveld K O, Pietsch W J, Ratkowski A J, Vager Z and Zabransky B J 1979 Role of excited electronic states in the interactions of fast (MeV) molecular ions with solids and gases *Phys. Rev.* A **20** 834–54
[17] Vager Z, Naaman R and Kanter E P 1989 Coulomb explosion imaging of small molecules *Science* **244** 426–31
[18] Ellert C, Stapelfeldt H, Constant E, Sakai H, Wright J, Rayner D M and Corkum P B 1998 Observing molecular dynamics with timed Coulomb explosion imaging *Phil. Trans. R. Soc.* A **356** 329–44
[19] Boll R *et al* 2022 X-ray multiphoton-induced coulomb explosion images complex single molecules *Nat. Phys.* **18** 423–8
[20] Song P, Wang X, Meng C, Dong W, Li Y, Lv Z, Zhang D, Zhao Z and Yuan J 2019 Dynamics of three-particle fragmentation of $(CO_2)_2^{3+}$ ions produced by intense femtosecond laser fields *Phys. Rev.* A **99** 053427
[21] Livshits E *et al* 2024 Symmetry-breaking dynamics of a photoionized carbon dioxide dimer *Nat. Commun.* **15** 6322
[22] Fan Y, Wu C, Xie X, Wang P, Zhong X, Shao Y, Sun X, Liu Y and Gong Q 2016 Three-body fragmentation dynamics of carbon-dioxide dimers induced by intense femtosecond laser pulses *Chem. Phys. Lett.* **653** 108–11
[23] Rajput J *et al* 2018 Native frames: Disentangling sequential from concerted three-body fragmentation *Phys. Rev. Lett.* **120** 103001
[24] Wu C *et al* 2013 Nonsequential and sequential fragmentation of CO_2^{3+} in intense laser fields *Phys. Rev. Lett.* **110** 103601
[25] Neumann N *et al* 2010 Fragmentation dynamics of CO_2^{3+} investigated by multiple electron capture in collisions with slow highly charged ions *Phys. Rev. Lett.* **104** 103201
[26] Chen L, Wang E, Zhao W, Gong M, Shan X and Chen X 2023 Fragmentation of SO_2^{q+} $(q = 2 - 4)$ induced by 1ke V electron collision *J. Chem. Phys.* **158** 054301
[27] Guillemin R *et al* 2015 Selecting core-hole localization or delocalization in CS_2 by photofragmentation dynamics *Nat. Commun.* **6** 6166
[28] Bhattacharyya S *et al* 2022 Two- and three-body fragmentation of multiply charged tribromomethane by ultrafast laser pulses *Phys. Chem. Chem. Phys.* **24** 27 631–644
[29] McManus J W *et al* 2022 Disentangling sequential and concerted fragmentations of molecular polycations with covariant native frame analysis *Phys. Chem. Chem. Phys.* **24** 22699–709
[30] Kaderiya B, 2021 Imaging photo-induced dynamics in halomethane molecules with coincident ion momentum spectroscopy *PhD Thesis* Kansas State University. (https://hdl.handle.net/2097/41294)
[31] Travnikova O *et al* 2024 X-ray-induced molecular catapult: Ultrafast dynamics driven by lightweight linkages *J. Phys. Chem. Lett.* **15** 11 883–890
[32] Nahon L, Svensson A and Morin P 1991 Experimental study of the 4*d* ionization continuum in atomic iodine by photoelectron and photoion spectroscopy *Phys. Rev.* A **43** 2328–37

[33] Forbes R, De Fanis A, Rolles D, Pratt S T, Powis I, Besley N A, Milosavljević A R, Nicolas C, Bozek J D and Holland D M P 2020 Photoionization of the I 4d and valence orbitals of methyl iodide *J. Phys. B: At. Mol. Opt. Phys.* **53** 155101
[34] Schmid G *et al* 2019 Reaction microscope endstation at FLASH2 *J. Synchrotron Radiat.* **26** 854–867
[35] Schlegel H B, Millam J M, Iyengar S S, Voth G A, Daniels A D, Scuseria G E and Frisch M J 2001 *Ab initio* molecular dynamics: Propagating the density matrix with gaussian orbitals *J. Chem. Phys.* **114** 9758–63
[36] Iyengar S S, Schlegel H B, Millam J M, Voth G A, Scuseria G E and Frisch M J 2001 *Ab initio* molecular dynamics: Propagating the density matrix with gaussian orbitals. ii. generalizations based on mass-weighting, idempotency, energy conservation and choice of initial conditions *J. Chem. Phys.* **115** 10 291–302
[37] Schlegel H B, Iyengar S S, Li X, Millam J M, Voth G A, Scuseria G E and Frisch M J 2002 *Ab initio* molecular dynamics: Propagating the density matrix with Gaussian orbitals. iii. comparison with born–oppenheimer dynamics *J. Chem. Phys.* **117** 8694–704
[38] Becke A D 1993 Density-functional thermochemistry. iii. the role of exact exchange *J. Chem. Phys.* **98** 5648–52
[39] Lee C, Yang W and Parr R G 1988 Development of the colle-salvetti correlation-energy formula into a functional of the electron density *Phys. Rev.* B **37** 785–9
[40] Vosko S H, Wilk L and Nusair M 1980 Accurate spin-dependent electron liquid correlation energies for local spin density calculations: a critical analysis *Can. J. Phys.* **58** 1200–11
[41] Stephens P J, Devlin F J, Chabalowski C F and Frisch M J 1994 Ab initio calculation of vibrational absorption and circular dichroism spectra using density functional force fields *J. Phys. Chem.* **98** 11 623–627
[42] Dunning T H and Hay P J 1977 *Modern Theoretical Chemistry* vol 3 H F Schaefer III (Plenum) pp 1–28
[43] Bergner A, Dolg M, Küchle W, Stoll H and Preuß H 1993 Ab initio energy-adjusted pseudopotentials for elements of groups 13–17 *Mol. Phys.* **80** 1431–41
[44] Frisch M J et al, Gaussian16 Revision C.01, 2016, gaussian Inc. Wallingford CT
[45] Maclot S *et al* 2013 Dynamics of glycine dications in the gas phase: Ultrafast intramolecular hydrogen migration versus coulomb repulsion *J. Phys. Chem. Lett.* **4** 3903–9
[46] Piekarski D G, Delaunay R, Maclot S, Adoui L, Martín F, Alcamí M, Huber B A, Rousseau P, Domaracka A and Díaz-Tendero S 2015 Unusual hydroxyl migration in the fragmentation of β-alanine dication in the gas phase *Phys. Chem. Chem. Phys.* **17** 16 767–778
[47] Kling N G *et al* 2019 Time-resolved molecular dynamics of single and double hydrogen migration in ethanol *Nat. Commun.* **10** 2813
[48] McDonnell M *et al* 2020 Ultrafast laser-induced isomerization dynamics in acetonitrile *J. Phys. Chem. Lett.* **11** 6724–9
[49] Rousseau P, Piekarski D G, Capron M, Domaracka A, Adoui L, Martín F, Alcamí M, Díaz-Tendero S and Huber B A 2020 Polypeptide formation in clusters of β-alanine amino acids by single ion impact *Nat. Commun.* **11** 3818
[50] Barreiro-Lage D, Bolognesi P, Chiarinelli J, Richter R, Zettergren H, Stockett M H, Carlini L, Diaz-Tendero S and Avaldi L 2021 Smart decomposition' of cyclic alanine-alanine dipeptide by VUV radiation: A seed for the synthesis of biologically relevant species *J. Phys. Chem. Lett.* **12** 7379–86
[51] Mishra D, LaForge A C, Gorman L M, Díaz-Tendero S, Martín F and Berrah N 2024 Direct tracking of h2 roaming reaction in real time *Nat. Commun.* **15** 6656
[52] Jones J E and Chapman S 1924 On the determination of molecular fields.—II. From the equation of state of a gas *Phil. Trans. R. Soc.* A **106** 463–77
[53] National Center for Biotechnology Information PubChem 2023 Diiodomethane ground state geometry *PubChem Identifier: CID* 6346 (available at: https://pubchem.ncbi.nlm.nih.gov/compound/diiodomethane#section=3D-Conformer)
[54] Blanksby S J and Ellison G B 2003 Bond dissociation energies of organic molecules *Acc. Chem. Res.* **36** 255–63
[55] Lindle D W, Kobrin P H, Truesdale C M, Ferrett T A, Heimann P A, Kerkhoff H G, Becker U and Shirley D A 1984 Inner-shell photoemission from the iodine atom in CH_3I *Phys. Rev.* A **30** 239–44